Brain Atlas for Glycoprotein Hormone Receptors at Single-Transcript Level

Vitaly Ryu[1,2], Anisa Gumerova[1,2], Funda Korkmaz[1,2], Seong Su Kang[3], Pavel Katsel[4], Sari Miyashita[1,2], Hasni Kannangara[1,2], Liam Cullen[1,2], Pokman Chan[5], Tanchun Kuo[1,2], Ashley Padilla[1,2], Samir Zaidi[6], Se-Min Kim[1,2], Maria I. New[7], Clifford J. Rosen[8], Ki A. Goosens[1,4], Tal Frolinger[1,2], Vahram Haroutunian[4], Keqiang Ye[9], Daria Lizneva[1,2], Terry F. Davies[1,2], Tony Yuen[1,2] and Mone Zaidi[1,2]

[1]Center for Translational Medicine and Pharmacology, Icahn School of Medicine at Mount Sinai, New York, NY 10029

[2]Department of Medicine and of Pharmacological Sciences, Icahn School of Medicine at Mount Sinai, New York, NY 10029

[3]Department of Pathology, Emory University School of Medicine, Atlanta, GA 30322

[4]Department of Psychiatry, Icahn School of Medicine at Mount Sinai, New York, NY 10029

[5]Alamak Biosciences, Beverly, MA 01915

[6]Memorial Sloan Kettering Cancer Center, New York, NY 10065

[7]Department of Pediatrics, Icahn School of Medicine at Mount Sinai, New York, NY 10029

[8]Maine Medical Center Research Institute, Scarborough, ME 04074

[9]Faculty of Life and Health Sciences, and Brain Cognition and Brain Disease Institute, Shenzhen Institute of Advanced technology, Chinese Academy of Sciences, Shenzhen, China

Corresponding Author: Mone Zaidi [email: mone.zaidi@mssm.edu]

Abbreviated title: Brain atlas of glycoprotein hormone receptors

Conflict of Interest: M.Z. is an inventor on issued patents on inhibiting FSH for the prevention and treatment of osteoporosis and obesity: United States: 8,435,948 (2013) and 11,034,761 (2021). M.Z. is also an inventor on pending patent application on composition and use of humanized monoclonal anti–FSH antibodies. These patents are owned by Icahn School of Medicine at Mount Sinai (ISSMS), and M.Z. would be recipient of royalties, *per* institutional policy. M.Z. and K.Y. are inventors of a pending patent application on the use of FSH as a target for preventing Alzheimer's disease. The latter patent is jointly owned by ISSMS and Emory University, and M.Z. and K.Y. would be recipient of royalties, *per* institutional policy. The other authors declare no competing financial interests. M.Z. also consults for Gershon Lehmann, Guidepoint and Coleman groups, and is Deputy Editor for e*Life* and Editor for *Marrow* (*Annals of The New York Academy of Sciences*)—both positions are compensated. None of the other authors have any conflicts.

Acknowledgements: Work at Icahn School of Medicine at Mount Sinai was performed at the Center for Translational Medicine and Pharmacology and was supported by U19 AG060917 to M.Z. and C.J.R.; R01 DK113627 to M.Z. and T.F.D.; R01 AG074092 and U01 AG073148 to T.Y and M.Z; and R01 AG071870 to S.-M.K., T.Y. and M.Z. M.Z. also thanks the Harrington Discovery Institute for the Innovator–Scholar Award. C.J.R. acknowledges support from the NIH (P20 GM121301).

ABSTRACT

There is increasing evidence that anterior pituitary hormones, traditionally thought to have unitary functions in regulating single endocrine targets, act on multiple somatic tissues, such as bone, fat, and liver. There is also emerging evidence for anterior pituitary hormone action on brain receptors in mediating central neural and peripheral somatic functions. Here, we have created the most comprehensive neuroanatomical atlas on the expression of TSHRs, LHCGRs and FSHRs. We have used RNAscope, a technology that allows the detection of mRNA at single-transcript level, together with protein level validation, to document *Tshr* expression in 173 and *Fshr* expression in 353 brain regions, nuclei and sub–nuclei identified using the *Atlas for the Mouse Brain in Stereotaxic Coordinates*. We also identified *Lhcgr* transcripts in 401 brain regions, nuclei and sub–nuclei. Complementarily, we used ViewRNA, another single-transcript detection technology, to establish the expression of *FSHR*s in human brain samples, where transcripts were co–localized in *MALAT1*–positive neurons. In addition, we show high expression for all three receptors in the ventricular region—with yet unknown functions. Intriguingly, *Tshr* and *Fshr* expression in the ependymal layer of the third ventricle was similar to that of the thyroid follicular cells and testicular Sertoli cells, respectively. TSHRs were expressed specifically in tanycytes. In contrast, *Fshr*s were localized to NeuN–positive neurons in the granular layer of the dentate gyrus in murine and human brain—both are Alzheimer's disease vulnerable regions. Our atlas thus provides a vital resource for scientists to explore the link between the stimulation or inactivation of brain glycoprotein hormone receptors on somatic function. New actionable pathways for human disease may be unmasked through further studies.

INTRODUCTION

There is increasing evidence that pituitary hormones traditionally thought of as 'pure' regulators of single physiological processes affect multiple bodily systems, either directly or *via* actions on brain receptors (1, 2). We established, for the first time, a direct action of thyroid–stimulating hormone (TSH) on bone and found that TSH receptor (TSHR) haploinsufficiency causes profound bone loss in mice (2). We also found that follicle–stimulating hormone (FSH), *hitherto* thought to solely regulate gonadal function, displayed direct effects on the skeleton to cause bone loss (3), and on fat cells, to cause adipogenesis and body fat accumulation (4). Likewise, we showed that hormones from the posterior pituitary, namely oxytocin and vasopressin, displayed direct, but opposing skeletal actions—effects that may relate to the pathogenesis of bone loss in pregnancy and lactation, and in chronic hyponatremia, respectively (5-8). To add to this complexity, and in addition to the poorly recognized ubiquity of pituitary hormone receptors, the ligands themselves, or their variants, are expressed widely. We find the expression of a TSHβ variant (TSHβv) in bone marrow macrophages, while oxytocin is expressed by both osteoblasts and osteoclasts (9-12). These studies have together shifted the paradigm from established unitary functions of pituitary hormones to an evolving array of yet unrecognized roles of physiologic and pathophysiologic importance.

There is a compelling body of literature to support the expression of oxytocin receptors in various brain regions, and their function in regulating peripheral actions, such as social behavior and satiety (5, 13). However, there is relatively scant information on the expression, and importantly, the function of the anterior pituitary glycoprotein hormone family of receptors, namely FSHR, TSHR and luteinizing hormone/human chorionic gonadotropin receptor (LHCGR). Discrete sites of the rat, mouse and human brain express receptors for these hormones, with several studies pointing to their relationship to neural functions, such as cognition, learning, neuronal plasticity, and sensory perception, as well as to neuropsychiatric disorders, including

affective disorders and neurodegeneration (14-21) (Table 1). In the light of such discoveries, the link between the stimulation of these receptors in the brain and the regulation of peripheral physiological processes needs further investigation.

Here, we use RNAscope—a cutting–edge technology that detects single RNA transcripts—to create the most comprehensive atlas of glycoprotein hormone receptors in mouse brain. This compendium of glycoprotein hormone receptors in concrete brain regions and sub–regions at a single-transcript level should allow investigators to study both peripheral and central effects of the activation of individual receptors in health and disease. Our identification of brain nuclei with the highest density for each receptor should also create a new way forward in understanding the functional engagement of receptor–bearing nuclei within a large–scale functional network.

RESULTS

Very little is known about the function(s) of anterior pituitary hormone receptors in the brain, except for isolated studies showing a relationship with cognition and affect (Table 1). We therefore used RNAscope to map the expression of *Tshr*, *Lhcgr* and *Fshr* in the mouse brain; immunofluorescence and qPCR to provide confirmatory evidence for *Tshr* and *Fshr* expression; and ViewRNA and qPCR to examine for *FSHR* expression in AD–vulnerable regions of the human brain. RNAscope, which allows the detection of single transcripts, uses ~20 pairs of transcript–specific double *Z*–probes to hybridize 10–µm–thick whole brain sections. Preamplifiers first hybridize to the ~28–bp binding site formed by each double *Z*–probe; amplifiers then bind to the multiple binding sites on each preamplifier; and finally, labeled probes containing a fluorescent molecule bind to multiple sites of each amplifier. RNAscope data was quantified on sections from coded mice. Each section was viewed and analyzed using CaseViewer 2.4 (3DHISTECH, Budapest, Hungary) or QuPath v.0.2.3 (University of Edinburgh,

UK). The *Atlas for the Mouse Brain in Stereotaxic Coordinates* (22) was used to identify every nucleus or sub–nucleus in which we manually counted *Tshr*, *Lhcgr* or *Fshr* transcripts in every tenth section using a tag feature. Repeat counting of the same section agreed within <2%. Receptor density was calculated by dividing transcript count by the total area (μm^2, ImageJ) of each region, nucleus or sub–nucleus. Photomicrographs were prepared using Photoshop CS5.1 (Adobe) only to adjust brightness, contrast and sharpness, to remove artifacts (i.e., obscuring bubbles), and to make composite plates.

*Tshr*s were detected bilaterally in 173 brain nuclei and sub–nuclei, in the following descending order of transcript densities: ventricular region, olfactory bulb, forebrain, hypothalamus, medulla, cerebellum, midbrain and pons, cerebral cortex, hippocampus and thalamus (Fig. 1A). Importantly, thyroid glands from $Tshr^{-/-}$ mice did not show a signal, proving probe specificity (Fig. 1B). *Tshr* expression in pooled brain samples was confirmed by qPCR (Fig. 1C). The hypothalamus and hippocampus expressed *Tshr*s, with hypothalamic expression being considerably higher (P<0.01) in females than in males. Furthermore, within other regions of the brain, highest *Tshr* densities were as follows: ependymal layer of the third ventricle (slightly higher than the thyroid follicular cells); VTT in the olfactory bulb; HDB in the forebrain; MTu in the hypothalamus; SolV in the medulla; PFl in the cerebellum; LDTg in midbrain and pons; DP in the cerebral cortex; DG in hippocampus; and PPT in the thalamus (Fig. 1D) (see Appendix for nomenclature). Raw transcript counts in each region and representative micrographs are shown in Supplementary Figs. 1 and 2, respectively.

For purposes of replicability, we employed a complementary approach to study brain *Tshr* expression—the *Tshr*–deficient mouse—in which exon 1 of the *Tshr* gene is replaced by a *Gfp* cassette. This reporter strategy allows for the *in vivo* display of *Tshr* locations using GFP immunoreactivity (GFP–ir) as a surrogate for *Tshr* expression (2). Of note is that the $Tshr^{+/-}$ (haploinsufficient) mouse has one *Tshr* allele intact with normal thyroid function but expresses

GFP *in lieu* of one lost allele. In contrast, the *Tshr*$^{+/+}$ mouse does not express GFP–ir because both *Tshr* copies are intact and is therefore our negative control.

Consistent with our RNAscope finding, profound GFP–ir was noted in the ependymal region of the third ventricle, mostly in NeuN–negative tanycytes, but with some neuronal localization (Fig. 1E). The SVZ of the lateral ventricles, and the SI, and dorsal and ventral BNST of the forebrain also showed GFP-ir, but immunoreactivity was much lower than the ependymal layer of the third ventricle (Fig. 1F). In all, while there was overall concordance between the two methodologies for high *Tshr*–expressing areas, GFP–ir was not detected in a number of *Tshr*–positive regions. This latter discrepancy most likely reflects the grossly lower sensitivity of immunohistochemical detection.

There is evidence that high LH levels in post–menopausal women correlate with a higher incidence of Alzheimer's disease (AD) (23, 24); that LHβ transgenic mice are cognitively impaired (25); that LH receptors (LHCGRs) are present in the hippocampus (26, 27); and that hCG induces cognitive deficits in rodents (28, 29). Thus, we mapped *Lhcgr*s in mouse brain to document expression in 401 brain nuclei and sub–nuclei. Probe specificity was established by a positive signal in testicular Leydig cells, and with an absent signal in juxtaposed Sertoli cells (Fig. 2A). Notably similar to *Tshr* transcripts, the ventricular regions displayed the highest transcript density (Fig. 2B). Among the brain divisions, the densities were as follows: OV in the ventricular region; SFO in the forebrain; PFI in the cerebellum; MiA in the olfactory bulb; SCO in the thalamus; PMD in the hypothalamus; MVPO in the medulla; DT in midbrain and pons; GrDG in the hippocampus; and SL in the cerebral cortex (Fig. 2C). Raw transcript counts in each region and representative micrographs are shown in Supplementary Figs. 3 and 4, respectively.

We recently reported the expression of FSHRs in mouse, rat and human brains, particularly in AD–vulnerable regions, including hippocampus and cortex (30). We also found

that FSH exacerbated AD–like neuropathology and cognitive decline in *3xTg*, *APP*/*PS1* and *APP*-KI mice, while the inhibition of FSH action rescued this phenotype. Most notably, shRNA–mediated knockdown of the *Fshr* in the hippocampus prevented the onset of AD–like features (30). Here, using RNAscope, we report the expression of *Fshr*s at the single–transcript resolution in 353 brain nuclei and sub–nuclei—and suggest that FSHRs in the brain may have roles beyond cognition. Probe specificity was established by a positive signal in testicular Sertoli cells, and an absent signal in juxtaposed Leydig cells and in the testes of *Fshr*$^{-/-}$ mice—as negative controls (Fig. 3A). Immunofluorescence confirmed the expression of FSHRs in NeuN–positive neurons, but not in GFAP–positive glial cells or IBA1–positive microglia (Fig. 3B).

Fshr transcript density was highest in the ventricular region, followed in descending order, by the cerebellum, olfactory bulb, hippocampus, cerebral cortex, medulla, midbrain and pons, forebrain, thalamus, and hypothalamus (Fig. 3C). Within each region, respectively, the highest transcript densities were as follows: ependymal layer of the third ventricle (slightly higher than the testicular Sertoli cells); PFI in the cerebellum; GrA in the olfactory bulb; GrDG in the hippocampus; AIV in the cerebral cortex; RMg in the medulla; MHb in the thalamus; IPDL in midbrain and pons; aci in the forebrain; and ArcL in the hypothalamus (Fig. 3D). Raw transcript counts in each region and representative micrographs are shown in Supplementary Figs. 5 and 6, respectively.

We used ViewRNA to examine the expression of *FSHR* transcripts in specific regions of the human brain (Fig. 4A). Expression was noted in neuronal cells co–expressing the non–coding RNA *MALAT1* in the GrDG—consistent with the RNAscope data in mouse brain—and in the parahippocampal cortex. This latter data is consistent with *FSHR* expression in a population of excitatory glutamatergic neurons noted in human brain by 10X single cell RNA–seq (Allen Brain Atlas). Affymetrix microarray analysis confirmed *FSHR* expression in the frontal, cingulate,

temporal, parietal and occipital sub–regions of human cortex in postmortem normal and AD brains (Fig. 4B). Interestingly, *FSHR* expression trended to be higher in the frontal cortex of the AD brains compared to that of unaffected brains (P=0.060). In all, the data suggest that, beyond a primary role in regulating cognition, brain FSHRs may have a wider role in the central regulation.

DISCUSSION

The past decade has witnessed the unravelling of non–traditional physiologic actions of anterior pituitary glycoprotein hormones, and hence, the unmasking of functional receptors in bone, fat, brain, and immune cells, among other organs (1, 3, 4, 31-34). We report here for the first time that *Tshr*s, *Lhcgr*s and *Fshr*s are expressed in multiple brain regions. The data provide new insights into the distributed central neural network of anterior pituitary hormone receptors, particularly in relation to their role in regulating the somatic tissue function. Specifically, we find a surprising and striking overlap in central neural distribution of the three receptors—with highest transcript densities in the ventricular regions. Furthermore, at least for the TSHR and FSHR, expression levels in ependymal layer of the third ventricle was similar to that of the thyroid follicular cells and testicular Sertoli cells, respectively. *Albeit* intriguing, this may suggest a primary role for these receptors in central neural regulation.

Among 173 *Tshr*–positive brain regions, sub–regions and nuclei, the tanycyte–containing ependymal layer of the third ventricle displayed the highest *Tshr* transcript number and density. This region is juxtaposed to the anterior pituitary that produces TSH in response to hypothalamic thyrotropin–releasing hormone (TRH). Furthermore, TSH has been reported to be expressed in the hypothalamus (35, 36). It is therefore possible that a yet uncharacterized central TSH–TSHR feedback circuit may directly regulate the hypothalamic–pituitary–thyroid

axis, thought solely to be controlled by thyroid hormones. To add to this complexity, thyroxine to triiodothyronine conversion occurs in tanycytes (37), which calls into question whether central TSH actions regulate thyroid hormone metabolism in these cells, and/or directly modulate hypothalamic TRH neuronal projections.

The forebrain and olfactory bulb also displayed abundant *Tshr* transcripts, with the highest density in the nucleus of the horizontal limb of the diagonal band (HDB) of the forebrain and ventral tenia tecta (VTT) of the olfactory bulb. These regions are involved, respectively, in learning and odor processing (38-42). In the hypothalamus, the highest density was found in medial tuberal nucleus (MTu), which controls ingestive behaviors and metabolism (43). Finally, we found more recently that the modulation of TSHRs in the bed nucleus of the stria terminalis (BNST), which receives direct afferents from the MTu (44), influences anxiety responses, suggesting that TSHR signaling might, in fact, mediate psychosocial behaviors.

While LH has a key role in reproduction and sexual development, we found 401 brain regions, sub–regions and nuclei expressing *Lhcgr*s. There were nominal differences in *Lhcgr* expression in many brain regions, but the ventricles stood out as having the highest *Lhcgr* density. Two regions deserve special mention. The *Lhcgr*–rich mitral cell layer of the accessory olfactory bulb (MiA) has a known role in scent communication during mating (45-48). A growing body of evidence suggests that men are attracted to cues of impending ovulation in women, raising an intriguing question on whether cycling hormones affect men's attraction and sexual behavior (45, 48). The broader question is whether LH surges in women during cycling may, in fact, alter male sexual behavior through central mechanisms. Second, a high *Lhcgr* density in the subfornical organ (SFO) of the forebrain was surprising. SFO sends efferent projections to the organum vasculosum of the lamina terminalis (OVLT) (49, 50), which is surrounded by GnRH neurons and contains estrogen receptors (ESRs) (51). We therefore speculate that

241 circumventricular interactions between LHCGRs, LH, GnRH, and ESR underpin the central
242 regulation of reproduction.

243 RNAscope revealed 353 *Fshr*–expressing brain regions, sub–regions and nuclei.
244 Highest expression was noted in the tanycyte–rich ependymal layer, not surprisingly given its
245 anatomical proximity to the anterior pituitary gland where FSH is produced in response to
246 hypothalamic gonadotropin–releasing hormone (GnRH). The functional significance of *Fshr*s
247 expressed in the cerebellum, particularly in the paraflocculus (PFI), is yet unknown. However,
248 other *Fshr*–high sub–regions, including the granular cell layer of the accessory olfactory bulb
249 (GrA), granular layer of the dentate gyrus (GrDG) and agranular insular cortex (AIV), have
250 known associations with odor processing, learning, memory formation and anticipation of
251 reward (52-54). It is possible that the anosmia of Kallman syndrome, with unclear etiology, may
252 arise from a dysfunctional FSHR–olfaction circuitry. We also find that inactivation of the
253 hippocampal *Fshr* blunts the cognitive impairment and AD–like neuropathology induced by
254 ovariectomy in *3xTg* mice. This data, together with gain– and loss–of–function studies suggest
255 that hippocampal and cortical FSHRs could represent therapeutic targets for AD.

256 In all, our results provide compelling evidence for multiple central nodes being targets of
257 the anterior pituitary glycoprotein hormones—a paradigm–shift that does not conform with the
258 dogma that pituitary hormones are solely master regulators of single bodily processes. Through
259 the intercession of emerging technologies, we compiled the most complete atlas of glycoprotein
260 hormone receptor distribution in the brain at a single–transcript resolution. In addition, we have
261 identified brain sites with the highest transcript expression and density, findings that are
262 imperative towards a better understanding of the neuroanatomical and functional basis of
263 pituitary hormone signaling in the brain. This understanding should provide the foundation for
264 innovative pharmacological interventions for a range of human diseases, wherein direct actions
265 of pituitary hormones, have been implicated, importantly, Alzheimer's disease.

METHODS

Mice

We used *Tshr*$^{+/-}$ (strain #004858, Jackson Laboratory), *Lhcgr*$^{-/-}$ (strain #027102, Jackson Laboratory), *Fshr*$^{-/-}$ mice (55) and their wild type littermates in this study. Adult male mice (~3 to 4–month–old) were housed in a 12 h:12 h light:dark cycle at 22 ± 2 ºC with *ad libitum* access to water and regular chow. All procedures were approved by the Mount Sinai Institutional Animal Care and Use Committee (approval number IACUC-2018-0047) and are in accordance with Public Health Service and United States Department of Agriculture guidelines.

RNAscope

Mouse brain tissue was collected for RNAscope. Briefly, mice were anesthetized with isoflurane (2 to 3 % in oxygen; Baxter Healthcare, Deerfield, IL) and transcardially perfused with 0.9% heparinized saline followed by 4% paraformaldehyde (PFA). Brains were extracted and post–fixed in 4 % PFA for 24 hours, dehydrated and embedded into paraffin. Coronal sections were cut at 5 µm, with every tenth section mounted onto ~20 slides with 2–6 sections on each slide. This method allowed to cover the entire brain and to eliminate the likelihood of counting the same transcript twice. Sections were air dried overnight at RT and stored at 4 °C until required.

Simultaneous detection of mouse *Tshr*, *Lhcgr* and *Fshr* was performed on paraffin sections using RNAscope 2.5 LS Multiplex Reagent Kit and RNAscope 2.5 LS Probes, namely Mm-TSHR, Mm-LHCGR and Mm-FSHR (Advanced Cell Diagnostics, ACD). RNAscope assays on thyroid glands and testes (positive controls for *Tshr* and *Lhcgr*/*Fshr*, respectively), as well as brains from knockout mice (negative controls), were performed in parallel.

Slides were baked at 60 °C for 1 hour, deparaffinized, incubated with hydrogen peroxide for 10 minutes at room temperature, pretreated with Target Retrieval Reagent for 20 minutes at 100 °C and with Protease III for 30 minutes at 40 °C. Probe hybridization and signal amplification were performed *per* manufacturer's instructions for chromogenic assays.

Following RNAscope assay, the slides were scanned at 20x magnification and the digital image analysis was successfully validated using the CaseViewer 2.4 (3DHISTECH, Budapest, Hungary) software. The same software was employed to capture and prepare images for the figures in the manuscript. Detection of *Tshr*–, *Lhcgr*– and *Fshr*–positive cells were also performed using the QuPath-0.2.3 (University of Edinburgh, UK) software based on receptor intensity thresholds, size and shape.

Histology and Immunofluorescence

Heterozygous *Tshr*$^{+/-}$ mice in which a GFP cassette replaced exon 1 of the *Tshr* gene and their *Tshr*$^{+/+}$ littermates were euthanized with carbon dioxide and perfused transcardially with 0.9 % heparinized saline followed by 4 % PFA in 0.1 M phosphate buffered saline (PBS; pH 7.4). Brains were collected and post–fixed in the same fixative for overnight at 4 °C, then transferred to a 30 % sucrose solution in 0.1 M PBS with 0.1 % sodium azide and stored at 4 °C until they were sectioned on a freezing stage sliding microtome at 30 µm. Sections were stored in 0.1 M PBS solution with 0.1 % sodium azide until processed for double immunofluorescence.

For the double-label fluorescent immunohistochemistry, free–floating brain sections were rinsed in 0.1 M PBS (2 x 15 min) followed by a 30 min blocking in 3 % normal horse serum (Vector Laboratories, Burlingame, CA) and 0.3 % Triton X-100 in 0.1 M PBS. Sections were incubated with a mixture of primary rabbit anti–GFP antibody (1:500; catalog #SP3005P, OriGene, Rockville, MD) and mouse anti–NeuN antibody (1:1000; catalog #ab104224, Abcam,

Cambridge, MA) for 18 h. Sections were then incubated with the secondary donkey anti–rabbit Alexa 488 (1:700; catalog #711-545-152, Jackson Immunoresearch, West Grove, PA) and donkey anti–mouse DyLight 594 (1:700; catalog #DK-2594, Vector Laboratories, Burlingame, CA) antibodies in 0.1 M PBS for 3 hours at room temperature. For immunohistochemical controls, the primary antibody was either omitted or pre–adsorbed with the immunizing peptide overnight at 4 °C resulting in no immunoreactive staining. In addition, we expectedly did not detect GFP immunoreactivity (-ir) in the *Tshr*$^{+/+}$ littermates, as the *Tshr* gene was intact and did not express GFP. Sections were mounted onto slides (Superfrost Plus) and cover–slipped using ProLong Gold Antifade Reagent (Life Technologies, Grand Island, NY). All steps were performed at room temperature.

For immunofluorescence staining for FSHR, free-floating brain sections were incubated overnight at 4 °C with primary anti-FSHR (1:200; catalog # PA5-50963, ThermoFisher), anti-NeuN (1:300; catalog #MAB377, Sigma-Aldrich), anti-GFAP (1:400; catalog #MAB360, Sigma-Aldrich) or anti-IBA1 (1:500; catalog # PA5-18039, ThermoFisher) antibodies. After washing with Tris-buffered saline, the sections were incubated with a mixture of labelled secondary antibodies for detection. DAPI (Sigma-Aldrich) was used for staining nuclei.

Microarray Analysis

Affymetrix Human Genome U133 Plus 2.0 Array data for *FSHR* expression in the frontal, cingulate, temporal, parietal and occipital cortex from both AD and non-AD human brains were curated from a previously published dataset (GEO accession #GSE84422) (56).

Quantitative PCR

For quantitative RT-PCR performed on homogenates of brain tissues, total RNA from the hypothalamus and the hippocampus isolated from five *Tshr*$^{+/+}$ mice was extracted using an RNeasy Mini kit (Qiagen) *per* manufacturer's protocol. Thyroid and the liver tissues were used as positive and negative controls, respectively. RNA was treated with DNAse I (Invitrogen), and reverse transcribed using the SuperScript II Reverse Transcriptase (Thermo Fisher Scientific). qPCR was performed with a QuantStudio 7 Real-Time PCR system (Applied Biosystems). PCR reaction mix consisted of first–strand cDNA template, exon-spanning primer pairs, and SYBR Green PCR master mix (Thermo Fisher Scientific). Expression of the selected targets was compared to that of a panel of normalizing genes (*Rps11*, *Tubg1* and *Gapdh*) measured on the same sample in parallel on the same plate, giving a Ct difference (ΔCt) for the normalizing gene minus the test gene. Relative expression levels were calculated by $2^{-\Delta\Delta Ct}$ using thyroid as the reference tissue.

Quantitation, Validation and Statistical Analysis

Immunofluorescent images were viewed and captured using 10x or 20x objectives with an Observer.Z1 fluorescence microscope (Carl Zeiss, Germany) with appropriate filters for Alexa 488, Cy3 and DAPI. The captured GFP and NeuN images were evaluated and overlaid using AxioVision v.4.8 software (Carl Zeiss, Germany) and ImageJ (NIH, Bethesda, MD).

Data were analyzed by two-tailed Student's *t*-test using Prism v.9.3.1 (Graphpad, San Diego, CA). Significance was set at $P < 0.05$.

DATA AVAILABILITY

All data generated or analyzed during this study are included in the manuscript and supporting files.

364 **Table 1: Known Functions of TSHR, FSHR and LHCGR in Brain.**

Receptor	Species	Brain Region	Possible Function	Reference
TSHR	Rat	Hypothalamus	Aging	(15)
	Mice	Hippocampus	Spatial learning and memory	(17)
	Rat	Hypothalamus, hippocampus, pyriform and postcingulate cortex	Thyroid regulation	(14)
	Rat	Hypothalamus	Feeding behavior	(57)
	Human	Hypothalamus, amygdala, cingulate gyrus, frontal cortex, hippocampus, thalamus	Mood disorders	(21)
	Quail	Hypothalamus	Seasonal reproduction	(32)
FSHR	Yak	Hypothalamus, pineal gland	Follicle growth, maturation, estrus	(58)
	Mice	Hippocampus	Mood regulation	(18)
LHCGR	Rat	Hypothalamus	Aging	(15)
	Mice	Hippocampus, cortex	Spatial memory, cognition, plasticity	(19)
	Rat	Hippocampus	Brain metabolism	(27)
	Fish	Hypothalamus	Functional roles	(59)
	Mice	Hippocampus	Promote Amyloid-β formation	(60)
	Mice	Cortex	Regulation of neurosteroid production	(20)
	Mice	Hypothalamus, hippocampus, midbrain, cortex	Regulation of reproductive functions	(61)
	Yak	Hypothalamus, pineal gland	Follicle growth, maturation, estrus	(58)
	Rat	Hypothalamus, hippocampus, dentate gyrus, cerebellum, brainstem, cortex	Cognitive function (AD)	(16)

365

366

367

REFERENCES

1. M. Zaidi *et al.*, Actions of pituitary hormones beyond traditional targets. *J Endocrinol* **237**, R83-R98 (2018).
2. E. Abe *et al.*, TSH is a negative regulator of skeletal remodeling. *Cell* **115**, 151-162 (2003).
3. L. Sun *et al.*, FSH directly regulates bone mass. *Cell* **125**, 247-260 (2006).
4. P. Liu *et al.*, Blocking FSH induces thermogenic adipose tissue and reduces body fat. *Nature* **546**, 107-112 (2017).
5. L. Sun *et al.*, Oxytocin regulates body composition. *Proc Natl Acad Sci U S A* **116**, 26808-26815 (2019).
6. L. Sun *et al.*, Functions of vasopressin and oxytocin in bone mass regulation. *Proc Natl Acad Sci U S A* **113**, 164-169 (2016).
7. R. Tamma *et al.*, Oxytocin is an anabolic bone hormone. *Proc Natl Acad Sci U S A* **106**, 7149-7154 (2009).
8. R. Tamma *et al.*, Regulation of bone remodeling by vasopressin explains the bone loss in hyponatremia. *Proc Natl Acad Sci U S A* **110**, 18644-18649 (2013).
9. G. Colaianni *et al.*, Regulated production of the pituitary hormone oxytocin from murine and human osteoblasts. *Biochem Biophys Res Commun* **411**, 512-515 (2011).
10. G. Colaianni *et al.*, Bone marrow oxytocin mediates the anabolic action of estrogen on the skeleton. *J Biol Chem* **287**, 29159-29167 (2012).
11. R. Baliram *et al.*, Thyroid and bone: macrophage-derived TSH-beta splice variant increases murine osteoblastogenesis. *Endocrinology* **154**, 4919-4926 (2013).
12. R. Baliram, R. Latif, S. A. Morshed, M. Zaidi, T. F. Davies, T3 Regulates a Human Macrophage-Derived TSH-beta Splice Variant: Implications for Human Bone Biology. *Endocrinology* **157**, 3658-3667 (2016).
13. T. L. Bale, A. M. Davis, A. P. Auger, D. M. Dorsa, M. M. McCarthy, CNS region-specific oxytocin receptor expression: importance in regulation of anxiety and sex behavior. *J Neurosci* **21**, 2546-2552 (2001).
14. P. Crisanti *et al.*, The expression of thyrotropin receptor in the brain. *Endocrinology* **142**, 812-822 (2001).
15. N. V. Emanuele, G. Baker, D. McDonald, L. Kirsteins, A. M. Lawrence, The impact of aging on luteinizing hormone (LH) and thyroid-stimulating hormone (TSH) in the rat brain. *Brain Res* **352**, 179-183 (1985).
16. Z. M. Lei, C. V. Rao, J. L. Kornyei, P. Licht, E. S. Hiatt, Novel expression of human chorionic gonadotropin/luteinizing hormone receptor gene in brain. *Endocrinology* **132**, 2262-2270 (1993).
17. S. Luan *et al.*, Thyrotropin receptor signaling deficiency impairs spatial learning and memory in mice. *J Endocrinol* **246**, 41-55 (2020).
18. W. K. Bi *et al.*, FSH signaling is involved in affective disorders. *Biochem Biophys Res Commun* **525**, 915-920 (2020).
19. J. A. Blair, S. Bhatta, G. Casadesus, CNS luteinizing hormone receptor activation rescues ovariectomy-related loss of spatial memory and neuronal plasticity. *Neurobiol Aging* **78**, 111-120 (2019).

20. P. M. Apaja, K. T. Harju, J. T. Aatsinki, U. E. Petaja-Repo, H. J. Rajaniemi, Identification and structural characterization of the neuronal luteinizing hormone receptor associated with sensory systems. *J Biol Chem* **279**, 1899-1906 (2004).
21. M. Naicker, S. Naidoo, Expression of thyroid-stimulating hormone receptors and thyroglobulin in limbic regions in the adult human brain. *Metab Brain Dis* **33**, 481-489 (2018).
22. G. Paxinos, K. B. J. Franklin, *The Mouse Brain in Stereotaxic Coordinates* (Academic Press, New York, ed. 3rd, 2007).
23. V. W. Henderson, A. Paganini-Hill, C. K. Emanuel, M. E. Dunn, J. G. Buckwalter, Estrogen replacement therapy in older women. Comparisons between Alzheimer's disease cases and nondemented control subjects. *Arch Neurol* **51**, 896-900 (1994).
24. W. A. Rocca *et al.*, Increased risk of cognitive impairment or dementia in women who underwent oophorectomy before menopause. *Neurology* **69**, 1074-1083 (2007).
25. G. Casadesus *et al.*, Increases in luteinizing hormone are associated with declines in cognitive performance. *Mol Cell Endocrinol* **269**, 107-111 (2007).
26. C. V. Rao, Involvement of Luteinizing Hormone in Alzheimer Disease Development in Elderly Women. *Reprod Sci* **24**, 355-368 (2017).
27. T. Liu, J. Wimalasena, R. L. Bowen, C. S. Atwood, Luteinizing hormone receptor mediates neuronal pregnenolone production via up-regulation of steroidogenic acute regulatory protein expression. *J Neurochem* **100**, 1329-1339 (2007).
28. A. Berry, Y. Tomidokoro, J. Ghiso, J. Thornton, Human chorionic gonadotropin (a luteinizing hormone homologue) decreases spatial memory and increases brain amyloid-beta levels in female rats. *Horm Behav* **54**, 143-152 (2008).
29. A. M. Barron, G. Verdile, K. Taddei, K. A. Bates, R. N. Martins, Effect of chronic hCG administration on Alzheimer's-related cognition and A beta accumulation in PS1KI mice. *Endocrinology* **151**, 5380-5388 (2010).
30. J. Xiong *et al.*, FSH blockade improves cognition in mice with Alzheimer's disease. *Nature* **603**, 470-476 (2022).
31. X. M. Liu *et al.*, FSH regulates fat accumulation and redistribution in aging through the Galphai/Ca(2+)/CREB pathway. *Aging Cell* **14**, 409-420 (2015).
32. G. R. Williams, Extrathyroidal expression of TSH receptor. *Ann Endocrinol (Paris)* **72**, 68-73 (2011).
33. D. Sun *et al.*, Roles of follicle stimulating hormone and its receptor in human metabolic diseases and cancer. *Am J Transl Res* **12**, 3116-3132 (2020).
34. M. J. Fields, M. Shemesh, Extragonadal luteinizing hormone receptors in the reproductive tract of domestic animals. *Biol Reprod* **71**, 1412-1418 (2004).
35. W. J. DeVito, T. N. Spearman, J. M. Connors, G. A. Hedge, Subcellular localization of immunoreactive thyroid-stimulating hormone in the rat hypothalamus. *Neuroendocrinology* **42**, 459-466 (1986).
36. S. Hojvat *et al.*, Immunoreactive thyroid stimulating hormone (TSH): association with synaptosomally-rich fractions in the rat hypothalamus. *Brain Res* **265**, 259-263 (1983).
37. T. L. Fonseca *et al.*, Coordination of hypothalamic and pituitary T3 production regulates TSH expression. *J Clin Invest* **123**, 1492-1500 (2013).

458 38. K. Shiotani *et al.*, Tuning of olfactory cortex ventral tenia tecta neurons to distinct
459 task elements of goal-directed behavior. *Elife* **9** (2020).
460 39. T. A. Cleland, C. Linster, Central olfactory structures. *Handb Clin Neurol* **164**, 79-
461 96 (2019).
462 40. A. M. McNamara, T. A. Cleland, C. Linster, Characterization of the synaptic
463 properties of olfactory bulb projections. *Chem Senses* **29**, 225-233 (2004).
464 41. I. Chaves-Coira, J. Martin-Cortecero, A. Nunez, M. L. Rodrigo-Angulo, Basal
465 Forebrain Nuclei Display Distinct Projecting Pathways and Functional Circuits to
466 Sensory Primary and Prefrontal Cortices in the Rat. *Front Neuroanat* **12**, 69
467 (2018).
468 42. X. Zhan, P. Yin, T. Heinbockel, The basal forebrain modulates spontaneous
469 activity of principal cells in the main olfactory bulb of anesthetized mice. *Front*
470 *Neural Circuits* **7**, 148 (2013).
471 43. S. X. Luo *et al.*, Regulation of feeding by somatostatin neurons in the tuberal
472 nucleus. *Science* **361**, 76-81 (2018).
473 44. H. W. Dong, L. W. Swanson, Projections from bed nuclei of the stria terminalis,
474 anteromedial area: cerebral hemisphere integration of neuroendocrine,
475 autonomic, and behavioral aspects of energy balance. *J Comp Neurol* **494**, 142-
476 178 (2006).
477 45. K. A. Gildersleeve, M. G. Haselton, C. M. Larson, E. G. Pillsworth, Body odor
478 attractiveness as a cue of impending ovulation in women: evidence from a study
479 using hormone-confirmed ovulation. *Horm Behav* **61**, 157-166 (2012).
480 46. K. Lydell, R. L. Doty, Male rat of odor preferences for female urine as a function
481 of sexual experience, urine age, and urine source. *Horm Behav* **3**, 205-212
482 (1972).
483 47. U. W. Huck, E. M. Banks, Social olfaction in male brown lemmings (Lemmus
484 sibiricus = trimucronatus) and collared lemmings (Dicrostonyx groenlandicus): I.
485 Discrimination of species, sex, and estrous condition. *J Comp Psychol* **98**, 54-59
486 (1984).
487 48. D. Singh, P. M. Bronstad, Female body odour is a potential cue to ovulation. *Proc*
488 *Biol Sci* **268**, 797-801 (2001).
489 49. R. R. Miselis, The efferent projections of the subfornical organ of the rat: a
490 circumventricular organ within a neural network subserving water balance. *Brain*
491 *Res* **230**, 1-23 (1981).
492 50. R. W. Lind, Bi-directional, chemically specified neural connections between the
493 subfornical organ and the midbrain raphe system. *Brain Res* **384**, 250-261 (1986).
494 51. M. J. Low, Neuroendocrinology: New hormone treatment for obesity caused by
495 POMC-deficiency. *Nat Rev Endocrinol* **12**, 627-628 (2016).
496 52. H. Eichenbaum, The hippocampus and declarative memory: cognitive
497 mechanisms and neural codes. *Behav Brain Res* **127**, 199-207 (2001).
498 53. S. Nagayama, R. Homma, F. Imamura, Neuronal organization of olfactory bulb
499 circuits. *Front Neural Circuits* **8**, 98 (2014).
500 54. R. P. Kesner, P. E. Gilbert, The role of the agranular insular cortex in anticipation
501 of reward contrast. *Neurobiol Learn Mem* **88**, 82-86 (2007).

55. A. Dierich *et al.*, Impairing follicle-stimulating hormone (FSH) signaling in vivo: targeted disruption of the FSH receptor leads to aberrant gametogenesis and hormonal imbalance. *Proc Natl Acad Sci U S A* **95**, 13612-13617 (1998).
56. M. Wang *et al.*, Integrative network analysis of nineteen brain regions identifies molecular signatures and networks underlying selective regional vulnerability to Alzheimer's disease. *Genome Med* **8**, 104 (2016).
57. J. R. Burgos, B. M. Iresjo, S. Warnaker, U. Smedh, Presence of TSH receptors in discrete areas of the hypothalamus and caudal brainstem with relevance for feeding controls-Support for functional significance. *Brain Res* **1642**, 278-286 (2016).
58. S. D. Huo *et al.*, Protein and mRNA expression of follicle-stimulating hormone receptor and luteinizing hormone receptor during the oestrus in the yak (Bos grunniens). *Reprod Domest Anim* **52**, 477-482 (2017).
59. C. Peng *et al.*, Cloning, expression and functional characterization of a novel luteinizing hormone receptor in the orange-spotted grouper, Epinephelus coioides. *Gen Comp Endocrinol* **267**, 90-97 (2018).
60. J. Lin *et al.*, Genetic ablation of luteinizing hormone receptor improves the amyloid pathology in a mouse model of Alzheimer disease. *J Neuropathol Exp Neurol* **69**, 253-261 (2010).
61. T. Hamalainen, M. Poutanen, I. Huhtaniemi, Age- and sex-specific promoter function of a 2-kilobase 5'-flanking sequence of the murine luteinizing hormone receptor gene in transgenic mice. *Endocrinology* **140**, 5322-5329 (1999).

FIGURE LEGENDS

Figure 1: *Tshr* Expression in the Mouse Brain. **(A)** *Tshr* transcript density in the thyroid and various brain regions detected by RNAscope. **(B)** RNAscope probe specificity is confirmed in the $Tshr^{+/+}$ thyroid. $Tshr^{-/-}$ thyroid was used as negative control. Scale bar: 50 µm. **(C)** *Tshr* expression in the mouse hypothalamus and hippocampus using quantitative PCR. The thyroid and the liver serve as positive and negative controls, respectively. Statistics: Mean ± s.e.m., N=4–5 mice/group, $^{**}P$<0.01. **(D)** *Tshr* transcript density in nuclei and sub-nuclei of the ventricular regions, olfactory bulb, forebrain, hypothalamus, medulla, cerebellum, midbrain & pons, cerebral cortex, hippocampus and thalamus. **(E)** Abundant GFP immunofluorescence (green) was detected in the ependymal layer of the third ventricle in $Tshr^{+/-}$ heterozygous mice, in which a GFP cassette replaced exon 1 of the *Tshr* gene. This GFP signal was absent in $Tshr^{+/+}$ mice. **(F)** GFP immunofluorescence was also detected in the subventricular zone (SVZ) of the lateral ventricle, and substantia innominata (SI) and dorsal and ventral bed nucleus of stria terminalis (BNST) in the forebrain of the $Tshr^{+/-}$ mice. Sections were co-stained with DAPI (blue) and a neuronal marker, NeuN (red). Scale bar: 100 µm.

Figure 2: *Lhcgr* Expression in the Mouse Brain. **(A)** RNAscope signals were detected in the Leydig cells, but not juxtaposed Sertoli cells, in the mouse testis, confirming probe specificity. Scale bar: 25 µm. **(B)** *Lhcgr* transcript density in the testis and various brain regions detected by RNAscope. **(C)** *Lhcgr* transcript density in nuclei and sub-nuclei of the ventricular regions, forebrain, cerebellum, olfactory bulb, thalamus, hypothalamus, medulla, midbrain & pons, hippocampus and cerebral cortex.

Figure 3: *Fshr* Expression in the Mouse Brain. **(A)** RNAscope signals were detected in the Sertoli cells, but not juxtaposed Leydig cells, in the mouse testis, confirming probe specificity.

552 Scale bar: 50 μm. **(B)** FSHR immunofluorescence (red) was colocalized with NeuN–positive
553 neurons, but not with GFAP–positive glial cells or IBA1–positive microglia. Scale bar: 100 μm
554 (magnified view, 10 μm). **(C)** *Fshr* transcript density in the testis and various brain regions
555 detected by RNAscope. **(D)** *Fshr* transcript density in nuclei and sub-nuclei of the ventricular
556 regions, cerebellum, olfactory bulb, hippocampus, cerebral cortex, medulla, midbrain & pons,
557 forebrain, thalamus and hypothalamus.
558
559 **Figure 4: *FSHR* Expression in the Human Brain.** **(A)** *FSHR* expression in the human
560 hippocampus and parahippocampal cortex was detected by ViewRNA in neuronal cells that
561 coexpress the non–coding RNA *MALAT1*. **(B)** *FSHR* mRNA expression in the frontal, cingulate,
562 temporal, parietal and occipital sub–regions of human cortex in postmortem normal and AD
563 brains (Affymetrix microarray, from GEO accession: GSE84422).
564
565 **Table 1: Known Functions of TSHR, FSHR and LHCGR in the Brain.**
566
567 **Supplementary Figure 1:** Raw *Tshr* transcript counts in each brain region, nuclei and
568 subnuclei.
569
570 **Supplementary Figure 2:** Representative RNAscope micrographs showing *Tshr* transcripts in
571 the ependymal layer of the third ventricle (3V), ventral tenia tecta (VTT) of the olfactory bulb,
572 nucleus of the horizontal limb of the diagonal band (HDB) of the forebrain, medial tuberal
573 nucleus (MTu) of the hypothalamus, solitary nucleus, ventral part (SolV) of the medulla,
574 paraflocculus (PFl) of the cerebellum, laterodorsal tegmental nucleus (LDTg) of the midbrain
575 and pons, dorsal peduncular cortex (DP) of the cerebral cortex, dentate gyrus (DG) of the
576 hippocampus, and posterior pretectal nucleus (PPT) of the thalamus. Scale bar: 50 μm.
577

Supplementary Figure 3: Raw *Lhcgr* transcript counts in each brain region, nuclei and subnuclei.

Supplementary Figure 4: Representative RNAscope micrographs showing *Lhcgr* transcripts in the olfactory ventricle (OV), subfornical organ (SFO) of the forebrain, paraflocculus (PFl) of the cerebellum, mitral cell layer of the accessory olfactory bulb (MiA), subcommissural organ (SCO) of the thalamus, premammillary nucleus, dorsal part (PMD) of the hypothalamus, medioventral periolivary nucleus (MVPO) of the medulla, dorsal terminal nucleus of the accessory optic tract (DT) of the midbrain and pons, granular layer of the dentate gyrus (GrDG) of the hippocampus, and semilunar nucleus (SL) of the cerebral cortex. Scale bar: 50 µm.

Supplementary Figure 5: Raw *Fshr* transcript counts in each brain region, nuclei and subnuclei.

Supplementary Figure 6: Representative RNAscope micrographs showing *Fshr* transcripts in the ependymal layer of the third ventricle (3V), paraflocculus (PFl) of the cerebellum, granule cell layer of the accessory olfactory bulb (GrA), granular layer of the dentate gyrus (GrDG) of the hippocampus, agranular insular cortex, ventral part (AIV) of the cerebral cortex, raphe magnus nucleus (RMg) of the medulla, interpeduncular nucleus, dorsolateral subnucleus (IPDL) of the midbrain and pons, anterior commissure, intrabulbar part (aci) of the forebrain, medial habenular nucleus (MHb) of the thalamus, and arcuate hypothalamic nucleus, lateral part (ArcL) of the hypothalamus. Scale bar: 50 µm.

Appendix: Glossary of the brain regions, nuclei and subnuclei.

Figure 1

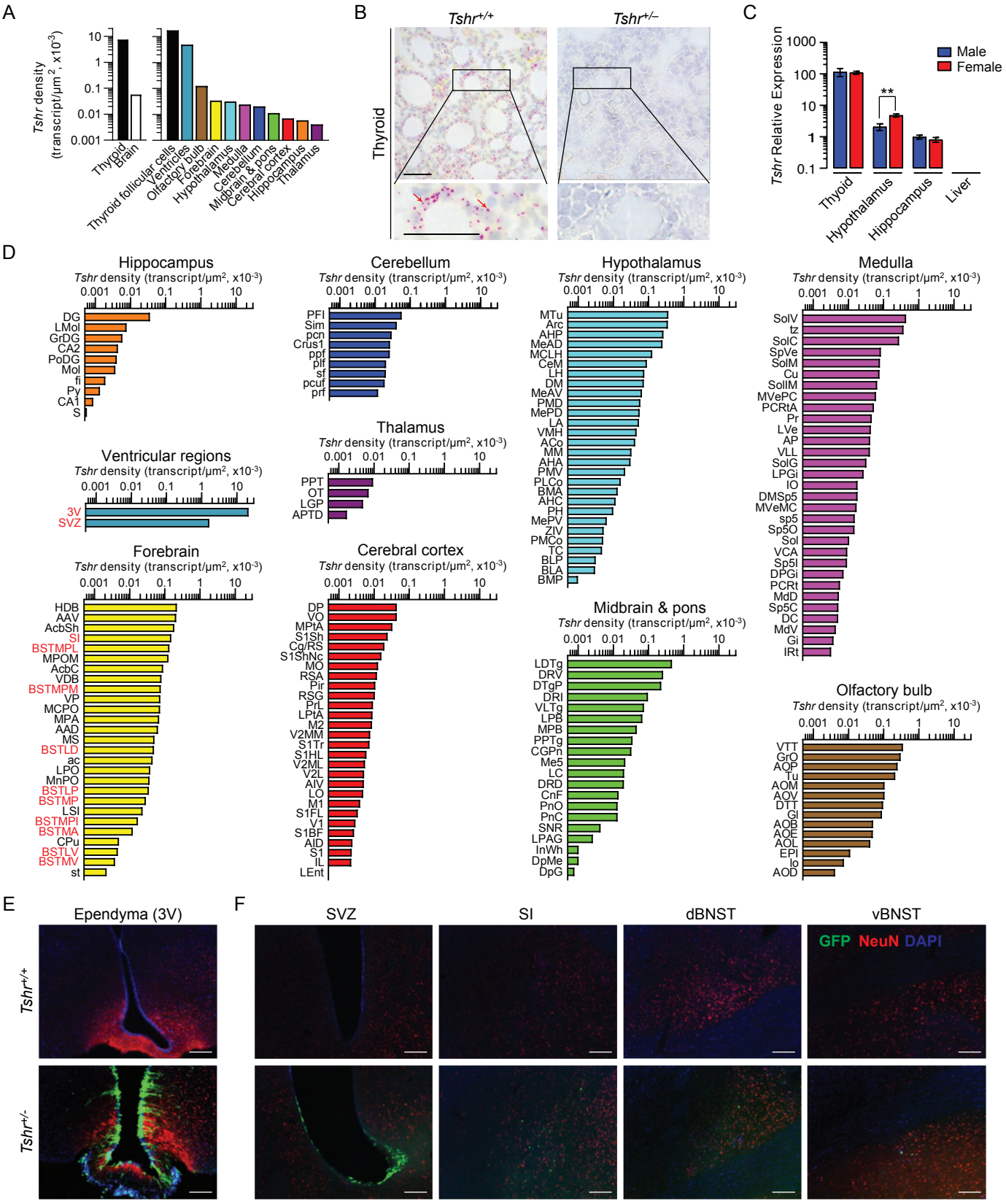

Figure 2

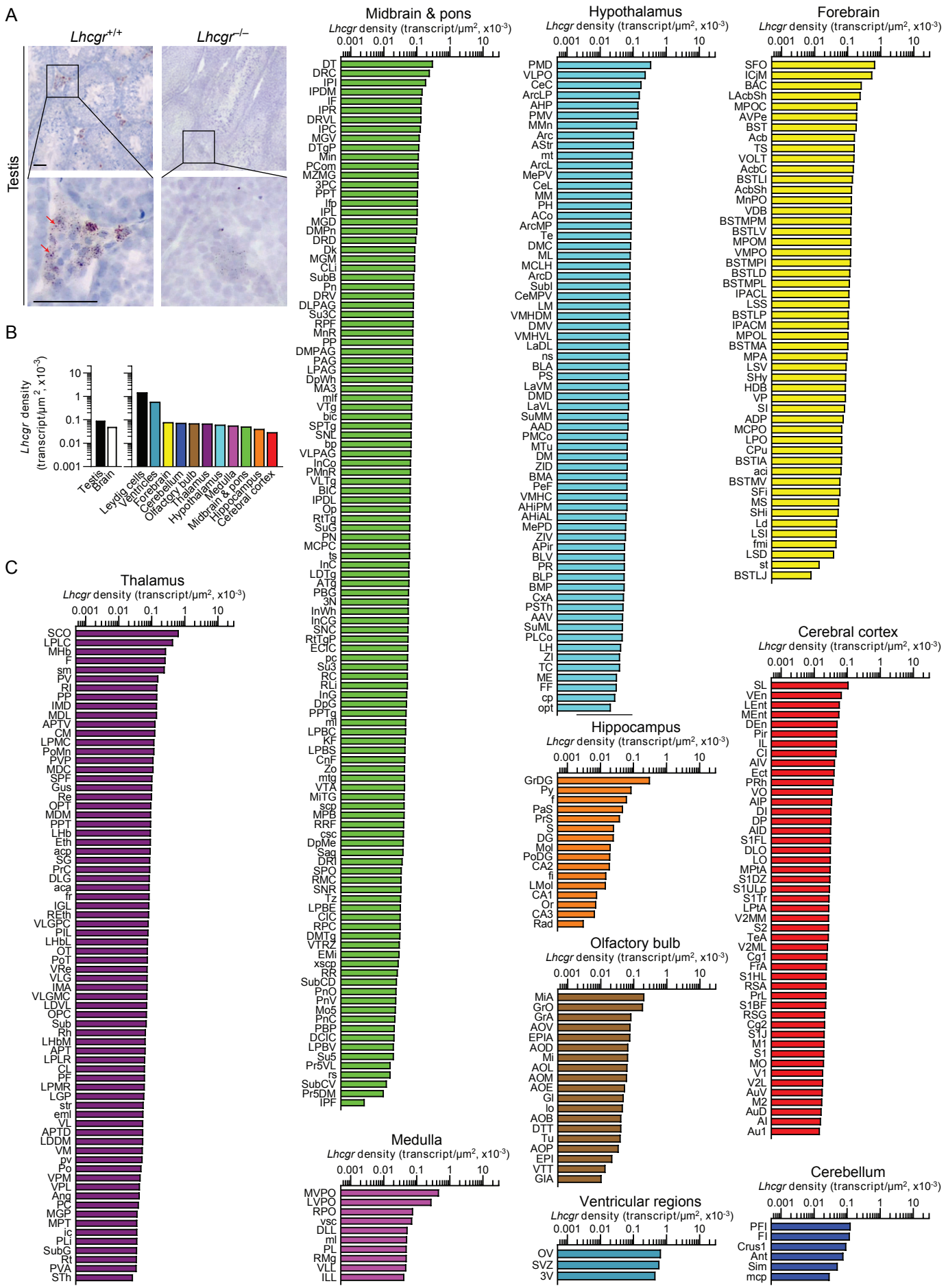

Figure 3

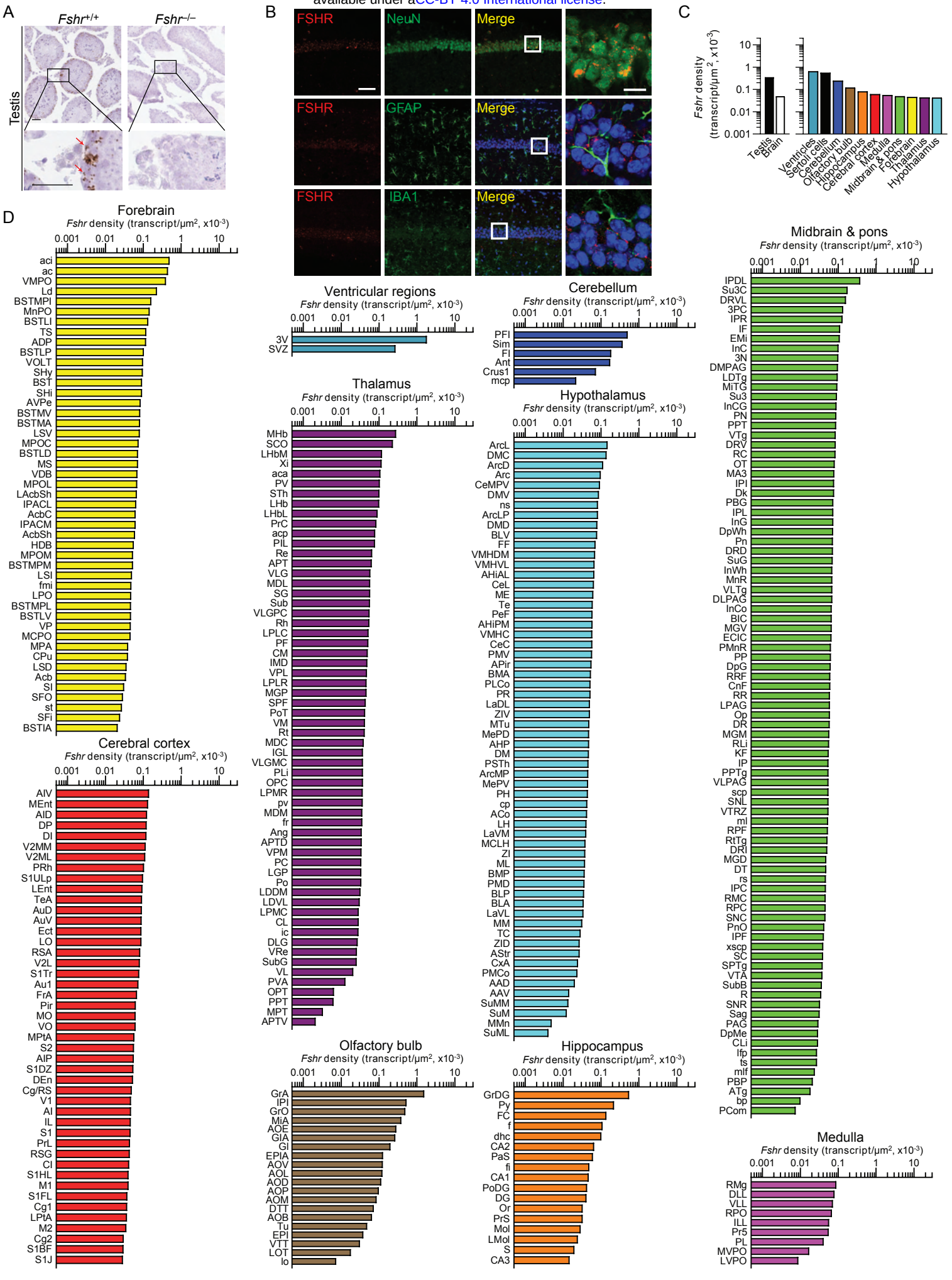

Figure 4

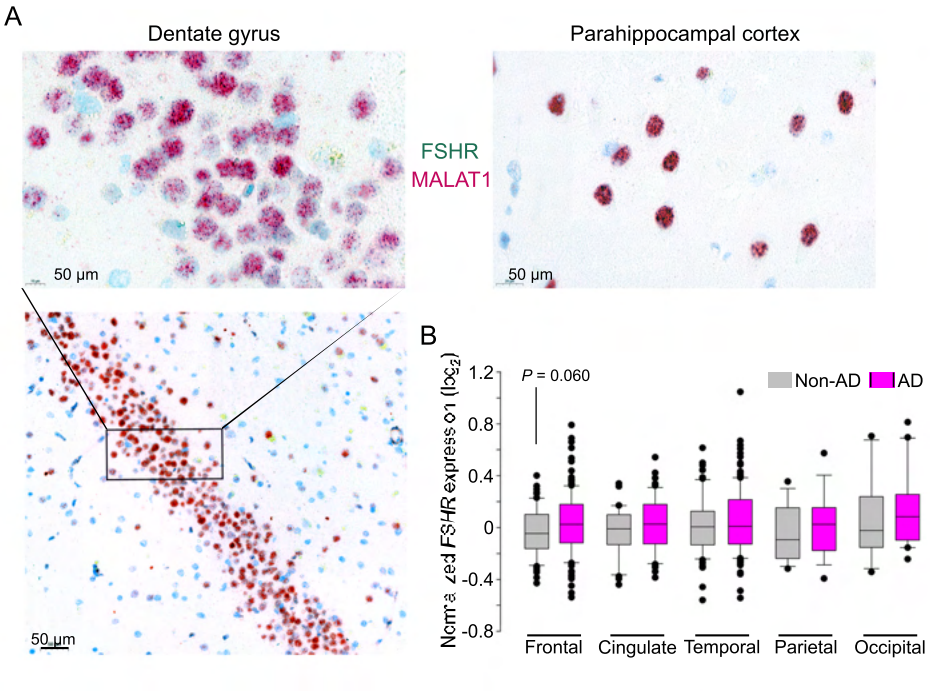

Supplementary Figure 1

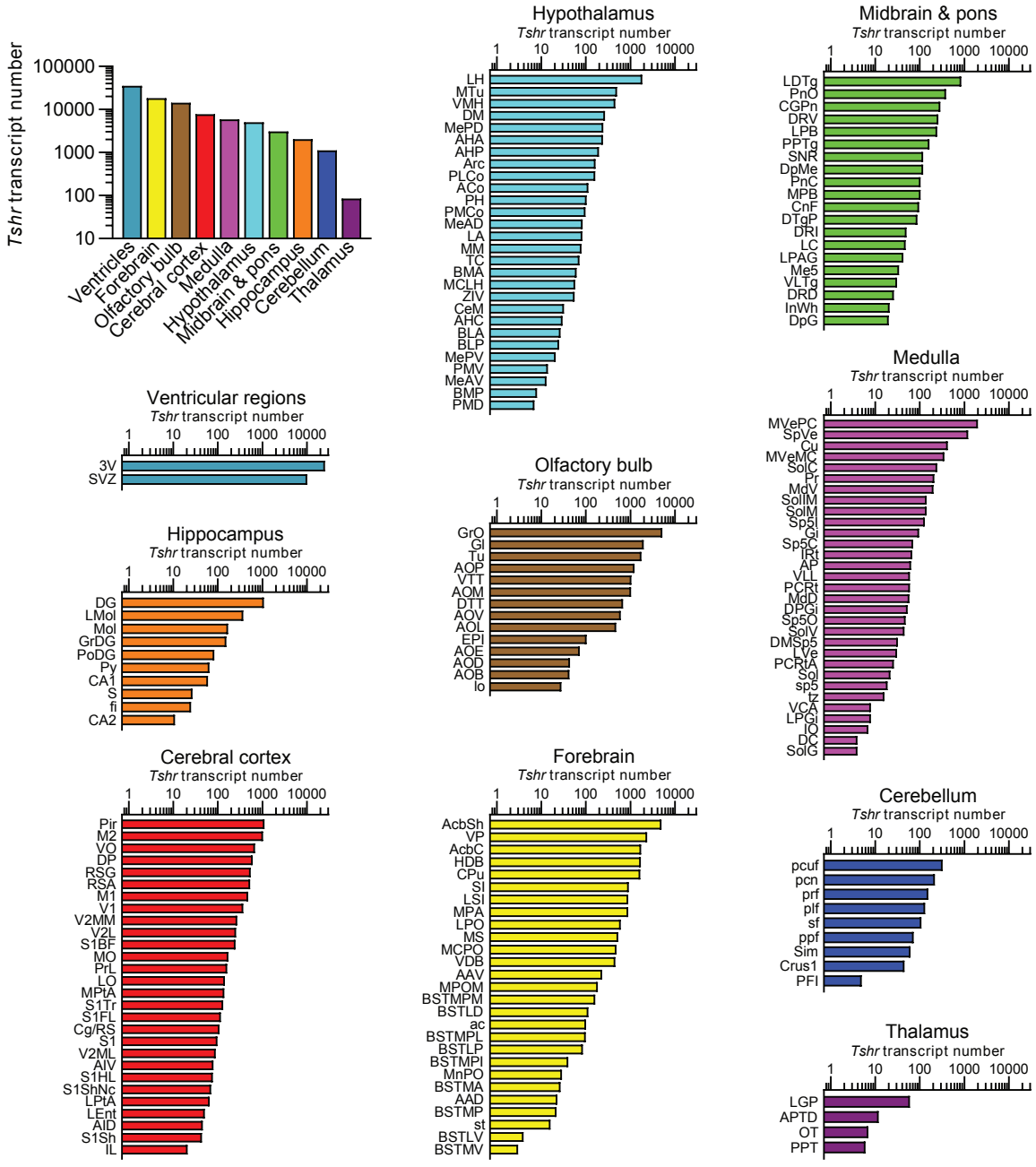

Supplementary Figure 2

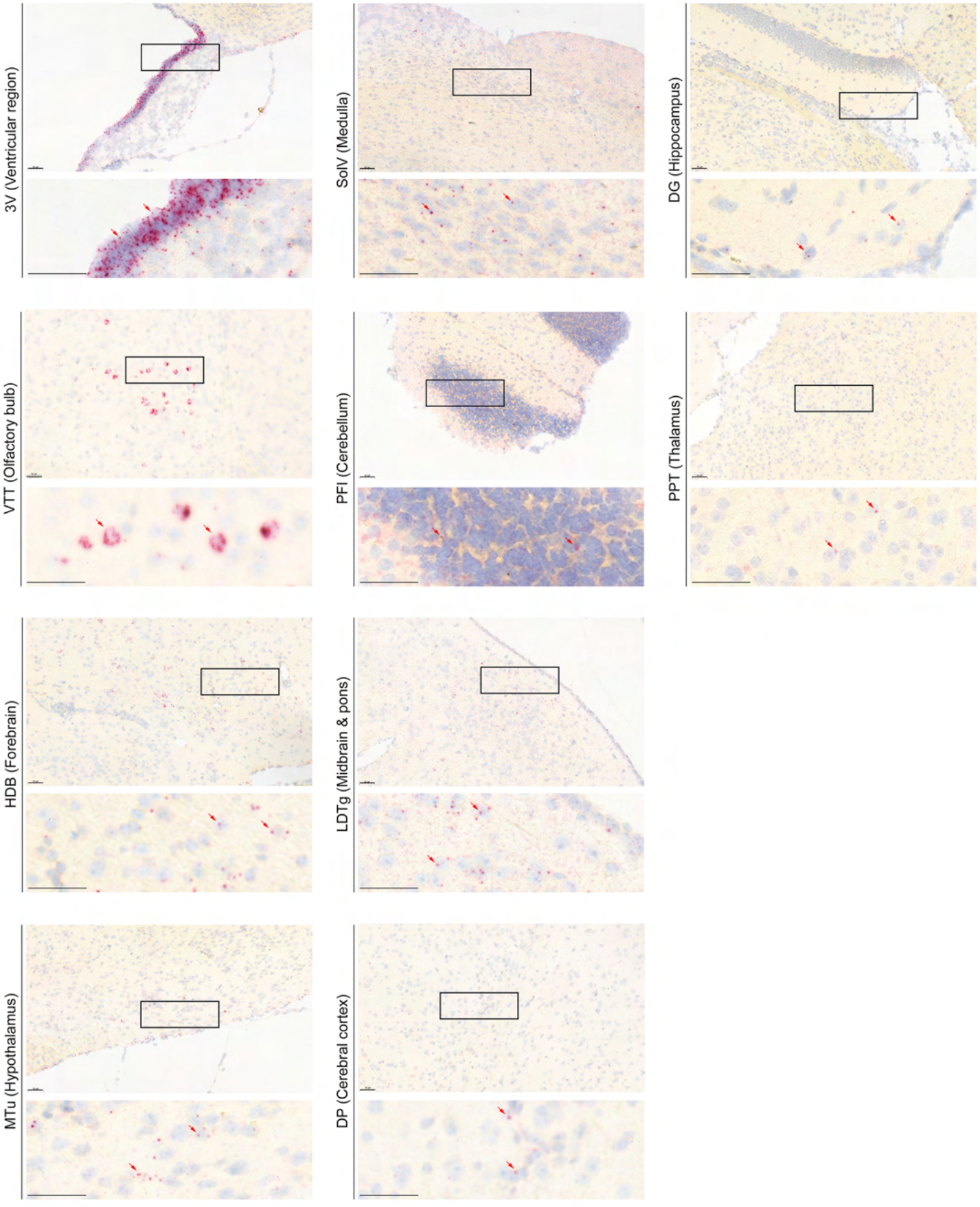

Supplementary Figure 3

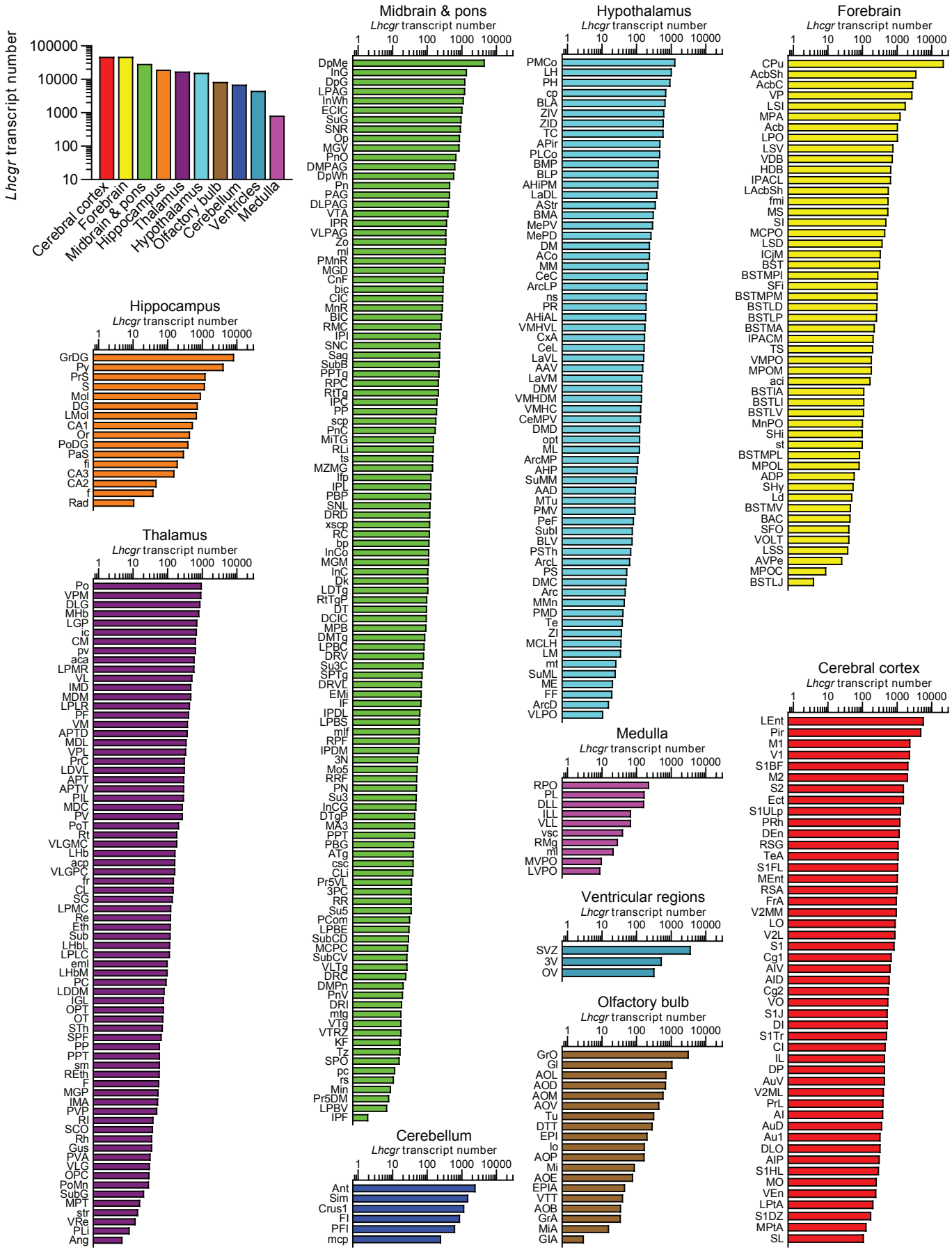

Supplementary Figure 4

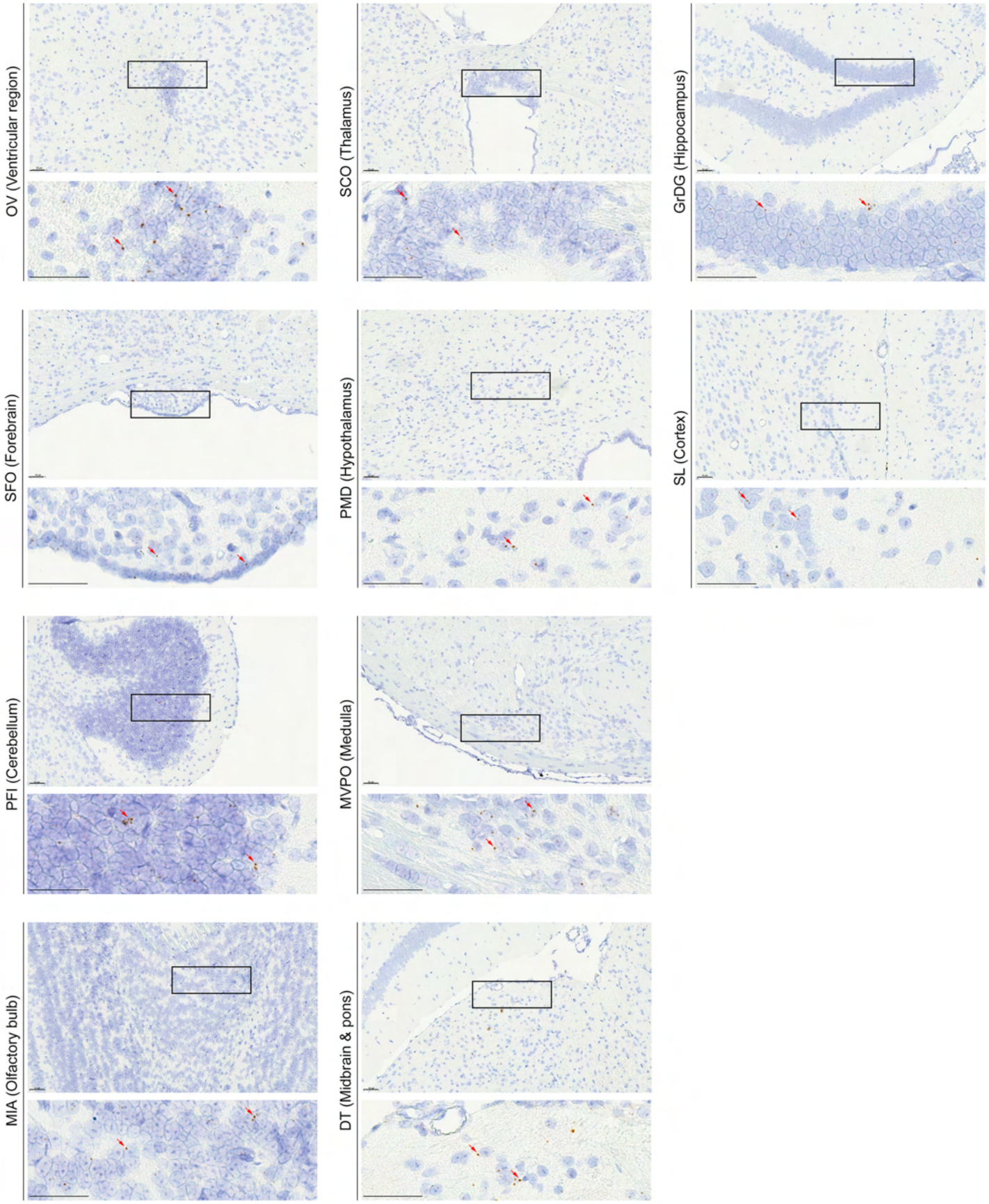

Supplementary Figure 5

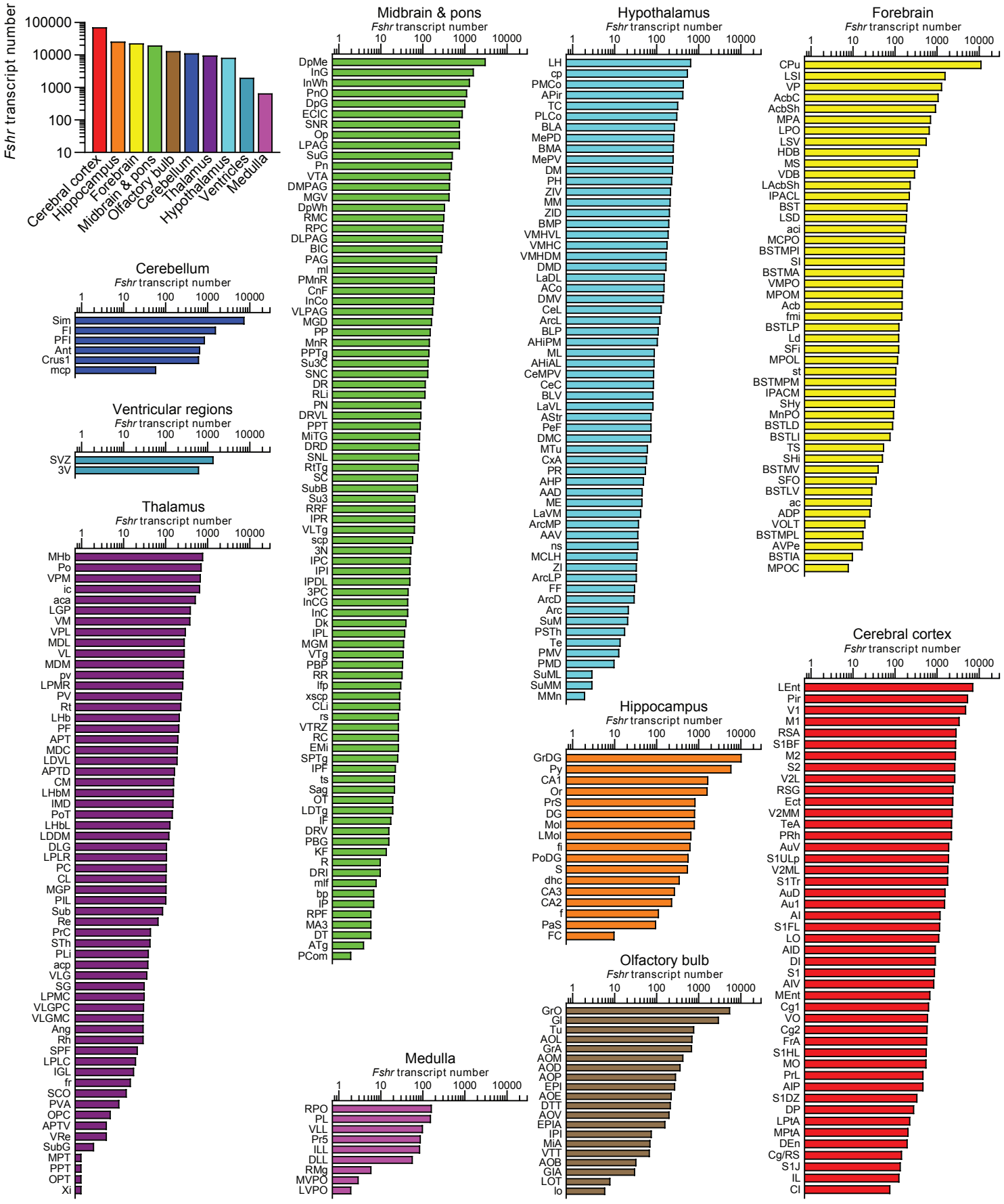

Supplementary Figure 6